

GNN-based Auto-Encoder for Short Linear Block Codes: A DRL Approach

Kou Tian, *Student Member, IEEE*, Chentao Yue, *Member, IEEE*, Changyang She, *Senior Member, IEEE*, Yonghui Li, *Fellow, IEEE*, and Branka Vucetic, *Life Fellow, IEEE*

Abstract—This paper presents a novel auto-encoder based end-to-end channel encoding and decoding. It integrates deep reinforcement learning (DRL) and graph neural networks (GNN) in code design by modeling the generation of code parity-check matrices as a Markov Decision Process (MDP), to optimize key coding performance metrics such as error-rates and code algebraic properties. An edge-weighted GNN (EW-GNN) decoder is proposed, which operates on the Tanner graph with an iterative message-passing structure. Once trained on a single linear block code, the EW-GNN decoder can be directly used to decode other linear block codes of different code lengths and code rates. An iterative joint training of the DRL-based code designer and the EW-GNN decoder is performed to optimize the end-end encoding and decoding process. Simulation results show the proposed auto-encoder significantly surpasses several traditional coding schemes at short block lengths, including low-density parity-check (LDPC) codes with the belief propagation (BP) decoding and the maximum-likelihood decoding (MLD), and BCH with BP decoding, offering superior error-correction capabilities while maintaining low decoding complexity.

Index Terms—Channel coding, Deep reinforcement learning, GNN, Auto-encoder

I. INTRODUCTION

The increasing demand for ultra-reliable low-latency communications (URLLC) in next-generation communication networks requires low-latency physical-layer designs – particularly channel coding schemes. Short codes with strong error-correction capability are essential to satisfy the stringent latency and reliability requirements of URLLC in 5G and future 6G networks [1], [2]. To meet these requirements, the channel coding system must demonstrate superior error-rate performance and low decoding complexity. This necessitates both a well-designed short channel code at the transmitter side and an efficient decoder at the receiver side.

Several short linear block codes, including Bose-Chaudhuri-Hocquenghem (BCH) codes, LDPC codes and Polar codes are promising candidates for URLLC due to their superior performance in the short block length regime [1]. Although long LDPC codes with the BP decoder have been adopted in the data channel of 5G new radio [3] due to their near-capacity performance and reasonable decoding complexity, their short variants suffer from a significant performance gap compared to the finite block length bound [4]. The suboptimal performance

of short LDPC codes primarily arises from the insufficient sparsity in the parity-check matrices, resulting in inherent limitations of the BP decoder, which exhibits a notable block-error-rate (BLER) performance degradation compared to MLD [1].

The conventional design of coding schemes involves dealing with a trade-off between BLER performance and decoding complexity. Such designs usually rely on the probabilistic and algebraic analyses. Due to the complexity of these analyses, the encoder and decoder are designed and optimized separately. Codes with high error-correction capabilities require complex decoding algorithms. For example, short BCH codes are among the best-known codes with strong error-correction performance, while their optimal decoding is highly computationally expensive [1]. On the other hand, LDPC paired with BP exhibits a significant BLER gap to the capacity bound, particularly at short block lengths [1].

Recently, there is a growing interest in leveraging artificial intelligence (AI) for wireless communication and channel coding [5], [6]. AI, particularly deep learning (DL), can potentially surpass analytical methods in the design of communication systems by learning the channel statistics, extracting features from wireless networks and exploring the optimal communication algorithms. AI-driven approaches have shown significant advantages in wireless system design and optimization, including signal detection [7] and channel resource allocation [8]. AI has also been integrated into code designs [9]–[12], decoder designs [13]–[20], and the joint optimization of encoding and decoding via end-to-end training [21]–[25]. The architecture that implements both the encoder and decoder with AI models is referred to as “auto-encoder” channel coding.

A. Related Works

1) *DL for Code Design*: The powerful capabilities of DL in data processing and feature learning offer a novel approach for constructing channel codes that can potentially outperform those designed by using human ingenuity [9]–[12]. In [9], [10], the authors used recurrent neural networks (RNNs) to construct low-latency and feedback codes, respectively, demonstrating performance gains. Authors in [11] proposed DL-based polar codes tailored to BP decoding, by treating the frozen positions of a polar code as trainable weights of a neural network. These works utilized existing code structures to ensure a manageable training complexity. Generally, learning to design linear block codes is challenging and faces several major challenges: 1) *Curse of dimensionality* [26]: As the message length k increases, the volume of the search space (i.e., the number of possible messages and codewords) increases exponentially as 2^k . Thus, the required number of training data becomes impractically large for supervised learning.

K. Tian, C. Yue, Y. Li, and B. Vucetic are with the School of Electrical and Computer Engineering, The University of Sydney, Sydney, Australia. C. She is with School of Electronic and Information Engineering, Harbin Institute of Technology (Shenzhen), Shenzhen, China. Part of this work was done when he was with the School of Electrical and Computer Engineering, The University of Sydney, Sydney, Australia. E-mails: {kou.tian, chentao.yue, yonghui.li, branka.vucetic}@sydney.edu.au, shechangyang@gmail.com

This paper was presented in part at IEEE International Conference on Communications (ICC), Rome, Italy, June 2023. This work has been supported by the SmartSat CRC, whose activities are funded by the Australian Government’s CRC Program.

Furthermore, a large k also results in high-dimensional input data, which leads to increased computational complexity. 2) *Gradient calculation*: Code matrices, i.e., the generator matrix and the parity-check matrix, are binary, which complicates the gradient calculation in the DL training process. 3) *Matrix validity*: Code matrices must be of full rank to ensure the code linearity, which introduces an extra constraint on the learning process. In [12], reinforcement learning (RL) was used to construct the binary code generator matrix in a systematic form. However, the designed codes exhibit limited error-rate performance.

2) *DL for Channel Decoding*: Recent works have achieved notable improvements in using DL-aided decoders to decode traditional analytically designed codes. Deep neural networks based on the structure of the existing decoding algorithms, such as BP, have been extensively explored. In [14] and [15], the authors proposed a neural BP (NBP) decoder, by unrolling the iterative structure of BP to a non-fully connected network with trainable weights. NBP outperforms the conventional BP in terms of BLER when decoding short BCH codes. The NBP decoder was further improved in [16] by integrating it with a hyper-graph network, and it was also enhanced by the pruning-based NBP in [17], which removes less-weighted neurons in the NBP network to obtain different parity-check matrices in each iteration. In addition, the loss functions for training NBP were refined in [18]. Motivated by the graph-based representation of codes using Tanner graphs, [19] proposed a GNN decoder for linear block codes, which demonstrates competitive BLER performance for LDPC and BCH codes. Although aforementioned DL-aided decoders have made significant progress, they have several limitations. Specifically, 1) their BLER performance gap to the optimal MLD remains significant; 2) they are not scalable to code length and code rate, requiring re-training when either changes; and 3) their performance highly depends on the hyper-parameters of neural networks, which are obtained by trial-and-error.

3) *Auto-Encoder*: The traditional coding system integrates individually optimized encoder and decoder, but this approach does not necessarily yield a globally optimal solution. Recently, DL has been used for the global optimization of “auto-encoder” channel coding systems with jointly designed encoder and decoder [21]–[25]. However, due to the high complexity of training end-to-end models and the aforementioned dimensionality problem, the application of auto-encoders is often limited to very small code sizes. For example, the auto-encoder proposed in [22] can only be utilized for codeword lengths up to 8. One solution is to design structured auto-encoder models aligning with specific code structures, such as convolutional auto-encoder (ConvAE) [23] and Turbo auto-encoder (TurboAE) [24], rather than using a direct black-box model as in [22]. ConvAE uses convolutional neural networks (CNN) for block codes, and TurboAE is a turbo code-like variant of ConvAE, utilizing multiple CNNs for interleaved encoding and iterative decoding. However, these methods cannot learn good codes at moderate-to-long lengths, offering only slight improvements over analytically designed codes. In [21], the authors proposed a neural belief propagation auto-encoder (NBP-AE), which uses trainable binary weights that represent the parity-check matrix to link the encoder

and decoder to enable end-to-end training. However, NBP-AE still has a significant BLER performance gap to the carefully designed encoder-decoder pairs, including BCH codes with its near MLD and irregular LDPC codes with BP.

B. Contributions

This paper proposes a GNN-DRL auto-encoder. First, we develop a DRL-based code designer that can learn better codes with superior error-control capabilities compared to conventional codes. Then, we develop an EW-GNN decoder. Finally, the DRL-based code designer and the EW-GNN decoder are jointly optimized and integrated into an auto-encoder channel coding framework. The main contributions of the paper are summarized as follows:

- *DRL-based code designer*: We introduce a DRL-based code designer that leverages GNNs to construct high-performance parity-check matrices for linear block codes. This approach formulates the process of generating matrices as a MDP, where a GNN-based agent directly operates within the parity-check matrix by treating it as a lattice graph. Our DRL-based method supports active explorations of the code space beyond given data samples, and the reward functions are designed to optimize critical code performance metrics, including girth, decoding bit error rate (BER), and the minimum Hamming distance (MHD).
- *Scalable GNN decoder*: We develop a novel EW-GNN decoder for short linear block codes. To simplify the selection of hyper-parameters, EW-GNN applies the *algorithmic alignment* framework [27] by designing a unique GNN that precisely matches the traditional BP decoding method and operates over Tanner graphs. Specifically, each variable node in EW-GNN is assigned a hidden embedding that is iteratively updated based on edge messages on the Tanner graph. Then, each edge message is assigned a “weight” determined by a fully-connected feed-forward neural network (FNN). The FNNs located on all edges share the same trainable parameters. By reducing the weights of unreliable edge messages generated from small cycles of Tanner graphs, EW-GNN significantly improves the BER compared to BP. Due to the intrinsic scalability properties of GNNs, the number of trainable parameters of EW-GNN does not change with the code length. Moreover, after the supervised training process with a given linear block code, it can be applied to other linear block codes with different rates and lengths.
- *Jointly-designed auto-encoder*: We present an auto-encoder framework that combines the proposed DRL-based code designer with the EW-GNN decoder, enabling the joint optimization of codes and their decoders. An iterative training scheme is applied to the proposed auto-encoder model. First, the DRL-based code designer designs the optimal code, using a reward function that minimizes the BER with an initial decoder, e.g., BP. Next, the EW-GNN decoder is trained for the designed code. In the next training iteration, a new code will be updated based on the BER reward from the EW-GNN decoder, and the decoder will be fine-tuned again for the new code. This training process will continue for several iterations.

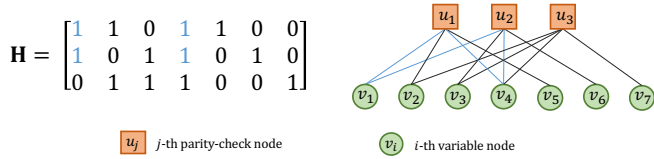


Fig. 1. A parity-check matrix in systematic form and its corresponding Tanner graph. The path marked by blue lines represents a 4-length cycle.

- We conducted extensive simulations to compare our code designer, decoder, and auto-encoder to conventional methods. The DRL-based code designer can discover better codes than LDPC codes under both BP and MLD decoders. Under MLD, the learned code has 0.83 dB more coding gain than the (32, 16) LDPC code on additive white Gaussian noise (AWGN) channels. Moreover, EW-GNN decoder outperforms BP and NBP in terms of BER, even when the code length in the training stage differs from that in the testing stage. For the (63, 51) BCH code, EW-GNN increases the coding gain by 1.2 dB and 0.62 dB compared to BP and NBP decoders, respectively. The proposed auto-encoder framework provides superior error-rate performance compared to multiple conventional encoder-decoder pairs and NBP-AE [21] at short block lengths. For example, our auto-encoder outperforms the (32, 16) LDPC decoded with MLD and BP by a coding gain of 0.63 dB and 1 dB, respectively.

The rest of this paper is organized as follows. Section II provides the preliminaries. In Section III, we introduce the DRL-based code designer. Section IV presents the EW-GNN decoder, outlining its structure and training algorithm. Section V presents the iterative training process of the proposed auto-encoder framework. In Section VI, we provide simulation results. Finally, Section VII concludes the paper.

II. PRELIMINARIES

A. Channel Coding with Linear Block Codes

We consider a binary linear block code denoted by $\mathcal{C}(n, k)$, where a k -bit binary message sequence is encoded into a codeword of length n with $n > k$.

1) *Matrix Representation*: For $\mathcal{C}(n, k)$, the encoding process can be succinctly represented by

$$\mathbf{c} = \mathbf{b}\mathbf{G}, \quad (1)$$

where $\mathbf{b} \in \mathbb{F}_2^k$ is the raw message, $\mathbf{c} \in \mathbb{F}_2^n$ is the codeword, and $\mathbf{G} \in \mathbb{F}_2^{k \times n}$ is the code generator matrix. Eq. (1) is performed over the binary field \mathbb{F}_2 . We denote the MHD of $\mathcal{C}(n, k)$ as d_{\min} .

The parity-check matrix of $\mathcal{C}(n, k)$ is denoted as $\mathbf{H} \in \mathbb{F}_2^{m \times n}$, where $m = n - k$. A parity-check matrix \mathbf{H} can be transformed into the systematic form as $\mathbf{H}_{\text{std}} = (\mathbf{A} \mid \mathbf{I}_m)$ through *Gaussian elimination*, where $\mathbf{A} \in \mathbb{F}_2^{m \times k}$ and \mathbf{I}_m is an identity matrix of size m . The associated systematic generator matrix can be accordingly obtained as $\mathbf{G}_{\text{std}} = (\mathbf{I}_k \mid \mathbf{A}^\top)$. Thus, \mathbf{G} and \mathbf{H} are both of full-rank, and either of them can fully define $\mathcal{C}(n, k)$.

2) *Graphical Representation*: As illustrated in Fig. 1, the Tanner graph of $\mathcal{C}(n, k)$ consists of two sets of nodes: n variable nodes corresponding to codeword bits and m check nodes corresponding to parity-check bits. The i -th variable node v_i is connected to the j -th check node u_j if the (j, i) -th element of

\mathbf{H} is one. In this case, \mathbf{H} can be interpreted as the adjacency matrix of a bipartite graph $\mathcal{G} = (\mathcal{V}, \mathcal{U}, \mathcal{E})$ with two disjoint node sets $\mathcal{V} = \{v_1, \dots, v_n\}$ and $\mathcal{U} = \{u_1, \dots, u_m\}$, and an edge set defined as $\mathcal{E} = \{e_{i,j} = (v_i, u_j) : v_i \in \mathcal{V}, u_j \in \mathcal{U}, H_{j,i} = 1\}$. We denote the neighborhood of a variable node v_i , i.e., all check nodes connected to v_i , as $\mathcal{M}(v_i) = \{u_j \in \mathcal{U} : e_{i,j} \in \mathcal{E}\}$. Similarly, $\mathcal{M}(u_j) = \{v_i \in \mathcal{V} : e_{i,j} \in \mathcal{E}\}$ represents the set of neighbor variable nodes of a check node u_j .

In the Tanner graph \mathcal{G} , a *cycle* of length λ (i.e., a λ -cycle) is a closed path that starts and ends at the same node, traversing λ edges in \mathcal{E} without repetition. The *girth* g of \mathcal{G} is the length of the shortest cycle. Since \mathcal{G} is bipartite, we have $g \geq 4$. The girth affects the decoding performance when using BP [28].

3) *Belief Propagation Decoding*: BP is a soft-decision decoding algorithm [29]. We denote the channel log-likelihood ratio (LLR) sequence of codeword \mathbf{c} as $\ell \in \mathbb{R}^n$. For the binary phase-shift keying (BPSK) modulation over an AWGN channel, ℓ_i can be obtained by

$$\ell_i = \ln \frac{\Pr(c_i = 0 \mid y_i)}{\Pr(c_i = 1 \mid y_i)} = \frac{2y_i}{\sigma_n^2}. \quad (2)$$

With ℓ , BP performs iterative message-passing decoding. Specifically, at the t -th iteration, it performs

$$\mu_{u_j \rightarrow v_i}^{(t)} = 2 \tanh^{-1} \left(\prod_{v \in \mathcal{M}(u_j) \setminus v_i} \tanh \left(\frac{\mu_{v \rightarrow u_j}^{(t-1)}}{2} \right) \right), \quad (3)$$

for each $u_j \in \mathcal{U}$ and $v_i \in \mathcal{M}(u_j)$, and

$$\mu_{v_i \rightarrow u_j}^{(t)} = \ell_i + \sum_{u \in \mathcal{M}(v_i) \setminus u_j} \mu_{u \rightarrow v_i}^{(t)}, \quad (4)$$

for each $v_i \in \mathcal{V}$ and $u_j \in \mathcal{M}(v_i)$. BP iteratively performs (3) and (4), until $\mu_{u_j \rightarrow v_i}^{(t)}$ and $\mu_{v_i \rightarrow u_j}^{(t)}$ converge, or the allowed maximum number of iterations is reached.

The BER of BP is strongly related to the girth g . Small cycles introduce correlations between messages passed across decoding iterations, thereby preventing the *a posteriori* LLR being exact [30]. For BCH codes and short LDPC codes, BP has inferior performance due to their small girths [1], [31].

B. Learning Approaches

1) *Reinforcement Learning*: RL is a trial-and-error approach to learn the optimal policy for sequential decision-making in dynamic environments. In RL, the decision-maker, known as the agent, performs actions in an environment and refines its behavior based on feedback received as rewards or penalties. A basic RL framework can be described by the MDP with components: State \mathbf{S}^t , Action \mathbf{A}^t , Policy μ , and Reward r . Precisely, policy determines actions in given states, i.e., $\mathbf{A}^t = \mu(\mathbf{S}^t)$. The reward evaluates action quality to guide the agent's behavior, which is given by $r^t = R(\mathbf{S}^t, \mathbf{A}^t, \mathbf{S}^{t+1})$ with a reward function R . In the agent-environment interaction loop, the agent takes an action \mathbf{A}^t based on the current policy μ and \mathbf{S}^t , then the system transits with a new state \mathbf{S}^{t+1} and receives a reward r^t . The goal of RL is to learn an optimal policy that can maximize the long-term reward, which is estimated by the action-value (Q-value) function in most RL algorithms.

In this work, we adopt the deep deterministic policy gradient (DDPG) algorithm [32], which is an actor-critic DRL method combining the strengths of the policy optimization method [33] and the Q-learning method [34]. It applies two deep

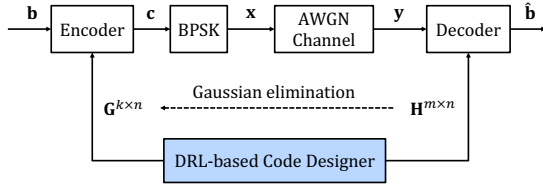


Fig. 2. System model.

neural networks to simultaneously learn a deterministic policy and an action-value function. The actor network determines the optimal actions, and the critic network estimates the Q-value, i.e., the long-term reward. DDPG has more stable and faster convergence than traditional RL by combining policy gradient for optimizing policies and Q-learning for value estimation.

2) *Graph Neural Network*: GNN is developed for processing graph structured data. It learns the low-dimensional representation of graphs, i.e., the network *embedding*, by iteratively propagating and aggregating the node/edge information over the graph [35]. Embeddings capture the graph topology, and have been used for graph analysis tasks, e.g., node/graph classification and link prediction [35].

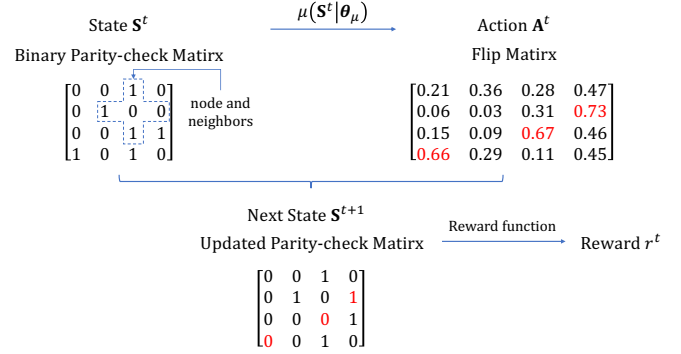
Message passing neural networks (MPNN) [36] have been successfully implemented in wireless communications [19], [37]. For a input graph, MPNN generates node embeddings through two neural network-based processes: the message calculation process and the embedding updating process. For each edge in the graph, a “message” is computed based on the node embeddings of its endpoints. Then, for each node, MPNN updates the embedding value by aggregating messages from its neighbors. Due to the graph-based nature of GNNs, the message calculation and the embedding updating can be applied to process the information flow on the Tanner graph, as demonstrated in the EW-GNN decoder (see Section IV-A). In the DRL-based code designer, the message calculation and the embedding updating are designed to operate on the lattice graph related to the parity-check matrix of a linear block code (see Section III-C).

III. CODE DESIGN WITH DRL

The enumeration algorithms to find short codes with the largest MHD [38] involve prohibitively high computational complexity, and the resulting codes often lack efficient decoding algorithms. To efficiently construct codes with superior error-correction performance and low decoding complexity, we propose a DRL-based code designer, which leverages DDPG to produce code parity-check matrices.

A. System Model

As demonstrated in Fig. 2, we consider a binary code $\mathcal{C}(n, k)$ defined by a parity-check matrix $\mathbf{H} \in \mathbb{F}_2^{m \times n}$, which is generated by the DRL-based code designer. Then, the corresponding generator matrix $\mathbf{G} \in \mathbb{F}_2^{k \times n}$ can be obtained by *Gaussian elimination*. A binary message \mathbf{b} is then encoded to a codeword \mathbf{c} following (1). We assume that \mathbf{c} is transmitted over the AWGN channel with the BPSK modulation. Thus, the modulated symbol \mathbf{x} is given by $\mathbf{x} = 1 - 2\mathbf{c} \in \{-1, 1\}^n$, and the noisy received signal \mathbf{y} is obtained as $\mathbf{y} = \mathbf{x} + \mathbf{z}$, where \mathbf{z} is the AWGN vector with each $z_i \sim \mathcal{N}(0, \sigma_n^2)$. The signal-to-noise ratio (SNR) is defined as $\text{SNR} = 1/\sigma_n^2$.


 Fig. 3. An example of the full graph-based MDP generating a parity-check matrix. The flipping threshold α_f is set as 0.5.

At the receiver side, a decoder processes \mathbf{y} and outputs an estimate $\hat{\mathbf{c}}$ of \mathbf{c} . The estimated message $\hat{\mathbf{b}}$ is the first k bits of $\hat{\mathbf{c}}$ when the generator matrix is systematic. A decoding error occurs when $\hat{\mathbf{b}} \neq \mathbf{b}$. The BER performance of the code defined by \mathbf{H} is calculated as:

$$\epsilon_b(\mathbf{H}) = \mathbb{E} \left[\frac{1}{k} \sum_{i=1}^k \mathbf{1}_{[b_i \neq \hat{b}_i]} \right], \quad (5)$$

where $\mathbf{1}_{[b_i \neq \hat{b}_i]} = 1$ if $b_i \neq \hat{b}_i$, and $\mathbf{1}_{[b_i \neq \hat{b}_i]} = 0$, otherwise. $\mathbb{E}[\cdot]$ is the expectation taken over random AWGN noise vectors.

B. Problem Formulation

The process of constructing parity-check matrices can be treated as a Tanner graph structure generation task. Intuitively, one can use a DRL agent to modify one edge at each time step, until all possible edges are updated. However, for the Tanner graph of $\mathcal{C}(n, k)$, the number of steps in each episode can be as high as $m \times n$, which leads to high training complexity. In addition, a reward is only available after the graph is fully generated. This issue is known as the *sparse reward* because the agent receives feedback only at the end of the entire episode, making it challenging to identify the impact of each individual action.

To address these issues, we consider a full graph-based MDP where in each step, the agent builds up a complete lattice graph of the whole parity-check matrix. Specifically, each matrix element is a node of the graph with links to its upper, lower, right, and left neighbouring elements. This graph is processed by GNN to produce actions, which will be further detailed in Section III-C. Figure 3 gives an example of the proposed iterative full graph-based MDP. Considering a linear block code $\mathcal{C}(n, k)$, a detailed description of the state representation, the action, and the reward function of the full graph-based MDP is as follows.

1) *States*: We define the state, \mathbf{S}^t , as the parity-check matrix at time step t , which is fully observed by the DRL agent. At the start of each episode, \mathbf{S}^1 is initialized by parity-check matrices from existing well-designed linear block codes [39].

2) *Actions*: We define a continuous, high-dimensional action space for link prediction. At each step t , the actor network determines the action $\mathbf{A}^t \in \mathbb{R}^{m \times n}$, with all elements scaled to

Algorithm 2: MPMNN $f_m(\mathbf{X} \mid \theta_m)$

Input : Feature matrix $\mathbf{X} \in \mathbb{R}^{m \times n \times d_0}$
Output: Embedding matrix $\hat{\mathbf{X}} \in \mathbb{R}^{m \times n \times d_e}$
 1 Initialize node embeddings by (11) for all node $(j, i) \in \mathbf{X}$
 for $l \leftarrow 1 : L$ **do**
 2 **foreach** $node (j, i) \in \mathbf{X}$ **do**
 3 Find embeddings of its neighbors;
 4 Compute messages by (10);
 5 Update its embedding by (9);
 6 **end**
 7 **endfor**

Algorithm 3: Actor Network $\mu(\mathbf{S}^t \mid \theta_\mu)$

Input : State $\mathbf{S}^t \in \mathbb{F}_2^{m \times n}$
Output: Action $\mathbf{A}^t \in \mathbb{R}^{m \times n}$
 1 Obtain $\mathbf{X}^a = \mathbf{S}^t \in \mathbb{R}^{m \times n \times 1}$;
 \triangleright Implement MPMNN with input \mathbf{X}^a ;
 2 Execute Algorithm 2;
 \triangleright Readout phase:
 3 **foreach** $node (j, i) \in \mathbf{X}^a$ **do**
 4 | Compute the action value by (12);
 5 **end**

where $\hat{\mathbf{x}}_{ji}^{l+1}$ is a d_e -dimensional vector. The parameterized function $f_e(\cdot \mid \theta_e)$ is a multilayer perceptron (MLP) with trainable parameters θ_e , working as the embedding updating function in a standard MPNN, and $\text{agg}(\cdot)$ is an aggregation function. For node (j, i) , $\mathbf{m}_{ji,l}^l, \mathbf{m}_{ji,r}^l, \mathbf{m}_{ji,u}^l, \mathbf{m}_{ji,d}^l$ are the messages passed from its neighbors in left, right, up and down directions at the l -th layer, and they are calculated as

$$\begin{aligned}
 \mathbf{m}_{ji,l}^l &= f_r(\hat{\mathbf{x}}_{ji}^l, \hat{\mathbf{x}}_{ji,l}^l \mid \theta_r), & \mathbf{m}_{ji,r}^l &= f_r(\hat{\mathbf{x}}_{ji}^l, \hat{\mathbf{x}}_{ji,r}^l \mid \theta_r), \\
 \mathbf{m}_{ji,u}^l &= f_c(\hat{\mathbf{x}}_{ji}^l, \hat{\mathbf{x}}_{ji,u}^l \mid \theta_c), & \mathbf{m}_{ji,d}^l &= f_c(\hat{\mathbf{x}}_{ji}^l, \hat{\mathbf{x}}_{ji,d}^l \mid \theta_c),
 \end{aligned} \tag{10}$$

where $\hat{\mathbf{x}}_{ji,l}^l, \hat{\mathbf{x}}_{ji,r}^l, \hat{\mathbf{x}}_{ji,u}^l, \hat{\mathbf{x}}_{ji,d}^l$ are embeddings of the neighbours of node (j, i) at the l -th layer. Note that $f_r(\cdot \mid \theta_r)$ and $f_c(\cdot \mid \theta_c)$ are two distinct MLPs to process incoming messages from same-row neighbors and same-column neighbors, respectively. These messages passed from neighbors are vectors of length d_m . At $l = 0$, we initialize embeddings for each node by applying a linear transformation

$$\hat{\mathbf{x}}_{ji}^0 = f_{in}(\mathbf{x}_{ji} \mid \theta_{in}), \tag{11}$$

where $f_{in}(\cdot \mid \theta_{in})$ is a dense layer that maps the d_0 -dimensional node into a d_e -dimensional embedding $\hat{\mathbf{x}}_{ji}^0$, and $d_e > d_0$.

The structure and flow of the MPMNN are summarised in Algorithm 2. As can be seen, the parameters of the MPMNN includes $\theta_e, \theta_r, \theta_c$, and θ_{in} in (9)-(11).

3) *Action Prediction and Critic Evaluation:* We apply two independent MPMNNs to construct the actor network and the critic network, denoted as $f_m^a(\mathbf{X}^a \mid \theta_m^a)$ and $f_m^c(\mathbf{X}^c \mid \theta_m^c)$, respectively. In the actor network $\mu(\mathbf{S}^t \mid \theta_\mu)$, \mathbf{S}^t is directly used as the input of $f_m^a(\cdot \mid \theta_m^a)$, i.e., $\mathbf{X}^a = \mathbf{S}^t \in \mathbb{R}^{m \times n \times 1}$ and $d_0 = 1$. After L layers, the readout phase computes the final action value based on the output embeddings, according to

$$A_{j,i}^t = \sigma(f_a(\hat{\mathbf{x}}_{ji}^L \mid \theta_a)), \tag{12}$$

where $f_a(\cdot \mid \theta_a)$ is a dense layer with inputs of dimension d_e and outputs of dimension one. The sigmoid function $\sigma(\cdot)$

Algorithm 4: Critic Network $Q(\mathbf{S}^t, \mathbf{A}^t \mid \theta_Q)$

Input : State $\mathbf{S}^t \in \mathbb{F}_2^{m \times n}$, action $\mathbf{A}^t \in \mathbb{R}^{m \times n}$
Output: Q-value q^t
 1 Obtain $\mathbf{X}^c = \text{concat}(\mathbf{S}^t, \mathbf{A}^t) \in \mathbb{R}^{m \times n \times 2}$;
 \triangleright Implement MPMNN with input \mathbf{X}^c ;
 2 Execute Algorithm 2;
 \triangleright Readout phase:
 3 Compute the Q-value q^t by (13).

is chosen to ensure that the action value is constrained within the range $(0, 1)$. The design of the actor network are detailed in Algorithm 3, where its parameter θ_μ is the subsumption of θ_m^a from $f_m^a(\mathbf{X}^a \mid \theta_m^a)$ and θ_a from (12).

In the critic network $Q(\mathbf{S}^t, \mathbf{A}^t \mid \theta_Q)$, the input of $f_m^c(\cdot \mid \theta_m^c)$ is given by $\mathbf{X}^c = \text{concat}(\mathbf{S}^t, \mathbf{A}^t) \in \mathbb{R}^{m \times n \times 2}$, where the concat operation combines \mathbf{S}^t and \mathbf{A}^t along the last dimension. Then we perform the MPMNN over this matrix. Following L layers, the readout phase calculates the Q-value by aggregating the embeddings of all nodes, as expressed by

$$q^t = \text{ReLU}(f_q(\text{agg}(\hat{\mathbf{x}}_{ji}^L : 1 \leq j \leq m, 1 \leq i \leq n) \mid \theta_q)), \tag{13}$$

where $f_q(\cdot \mid \theta_q)$ denotes a dense layer that transforms inputs of size d_e into a single-dimensional output. To obtain non-negative Q-values, we use the rectified linear unit (ReLU) as the activation function. The steps to compute the output of the critic network are summarized in Algorithm 4, where its parameter θ_Q is the subsumption of θ_m^c from $f_m^c(\mathbf{X}^c \mid \theta_m^c)$ and θ_q from (13).

D. Training Algorithm

The training process of the DRL-based code designer follows the algorithm detailed in Algorithm 5. During the training phase, we identify the optimal code by selecting the generated parity-check matrix, represented as \mathbf{H}^* , which is the state \mathbf{S}^{t+1} that yields the highest reward.

At each time step t , the agent observes the current state \mathbf{S}^t and generates an action by applying the actor network in Algorithm 3. To improve the exploration efficiency in our policy, we introduce noise to the actions during the training phase. The final action \mathbf{A}^t is given by

$$\mathbf{A}^t = \text{clip}(\tilde{\mathbf{A}}^t + \zeta, \alpha_{\text{low}}, \alpha_{\text{high}}), \tag{14}$$

where $\tilde{\mathbf{A}}^t = \mu(\mathbf{S}^t \mid \theta_\mu)$ is the output of Algorithm 3. The exploration noise ζ is sampled from a mean-zero Gaussian distribution. Considering the exploration-exploitation trade-off in RL, we design an epsilon-greedy noise selection method, in which ζ is added to the action with a decaying probability ϵ . Once ζ is added, ϵ is decayed to $\epsilon = 0.995\epsilon$ with a decaying rate 0.995, and ϵ is initialized to be 1. The variance of the Gaussian noise, σ_ϵ^2 , is chosen to be close to the flipping threshold in (6). The clip function then limits each element in the noised action $\tilde{\mathbf{A}}^t + \zeta$ to $[\alpha_{\text{low}}, \alpha_{\text{high}}]$.

After taking a certain action \mathbf{A}^t , the agent receives a reward r_t and observes a new state \mathbf{S}^{t+1} according to (6). The transition tuple $(\mathbf{S}^t, \mathbf{A}^t, r^t, \mathbf{S}^{t+1})$ is stored in a replay buffer \mathcal{D} , which is a finite sized cache. At each time step, a minibatch of size N_B is uniformly selected from the buffer and used as training samples to optimize the actor and critic networks. The

Algorithm 5: The DRL-Based Code Designer

Input : State initialization matrix \mathbf{S}^1 , reward function $R(\mathbf{S}^t, \mathbf{A}^t, \mathbf{S}^{t+1})$, number of steps T_c

Output: parity-check matrix \mathbf{H}^*

- 1 Initialize the critic network $Q(\cdot | \theta_Q)$ and $\mu(\cdot | \theta_\mu)$ with random parameters θ_Q and θ_μ ;
- 2 Initialize target networks by $\theta_{Q'} \leftarrow \theta_Q, \theta_{\mu'} \leftarrow \theta_\mu$;
- 3 Initialize $r_{max} = 0$ and an empty replay buffer \mathcal{D} ;
- 4 **foreach** *episode* **do**
- 5 Initialize the environment state \mathbf{S}^1 ;
- 6 **for** $t \leftarrow 1 : T_c$ **do**
- 7 Select action \mathbf{A}^t by (14), based on current state \mathbf{S}^t ;
- 8 Observe the new state \mathbf{S}^{t+1} by (6);
- 9 Evaluate reward r^t according to Algorithm 1;
- 10 **if** $r^t > r_{max}$ **then**
- 11 $\mathbf{H}^* = \mathbf{S}^{t+1}$;
- 12 $r_{max} = r^t$;
- 13 **end**
- 14 Store the transition $(\mathbf{S}^t, \mathbf{A}^t, r^t, \mathbf{S}^{t+1})$ in \mathcal{D} ;
- 15 **if** $size(\mathcal{D}) \geq N_B$ **then**
- 16 Randomly sample a batch of N_B transitions from \mathcal{D} ;
- 17 Update θ_Q by minimizing the loss in (15);
- 18 Update θ_μ by minimizing the loss in (18);
- 19 Update $\theta_{Q'}$ and $\theta_{\mu'}$ by (17);
- 20 **end**
- 21 **endfor**
- 22 **end**

optimization of the critic network is performed by minimizing the following loss function:

$$L(\theta_Q) = \frac{1}{N_B} \sum_{n_B=1}^{N_B} [y^t - Q(\mathbf{S}^t, \mathbf{A}^t | \theta_Q)]^2. \quad (15)$$

The loss is defined as the difference of the Q-value and the target value y^t , where the Q-value is obtained by Algorithm 4, and the target value y^t is computed according to Bellman equation [41]:

$$y^t = r^t + \gamma Q'(\mathbf{S}^{t+1}, \mu'(\mathbf{S}^{t+1} | \theta_{\mu'}) | \theta_{Q'}), \quad (16)$$

where $\gamma \in [0, 1]$ is a discounting factor. The target networks, $\mu'(\cdot | \theta_{\mu'})$ and $Q'(\cdot | \theta_{Q'})$, are replicas of the actor and critic networks, respectively. The parameters of target networks are updated according to,

$$\begin{aligned} \theta_{Q'} &\leftarrow \rho \theta_{Q'} + (1 - \rho) \theta_{Q'}, \\ \theta_{\mu'} &\leftarrow \rho \theta_{\mu'} + (1 - \rho) \theta_{\mu'}, \end{aligned} \quad (17)$$

and where $0 < \rho \ll 1$ is a hyper-parameter. Meanwhile, the optimal policy is trained by maximizing the Q-value function,

$$L(\theta_\mu) = -\frac{1}{N_B} \sum_{n_B=1}^{N_B} Q(\mathbf{S}^t, \mu(\mathbf{S}^t | \theta_\mu) | \theta_Q). \quad (18)$$

During the training phase, the parameters of the actor and critic networks are updated utilizing the Adam optimizer [42] with given learning rates η_a and η_c , respectively.

IV. EW-GNN DECODER

GNN is capable of learning well a wide range of practical models based on graphs, which is justified by the *algorithmic alignment* framework [27]. GNN can align to the BP decoding algorithm, because 1) BP decoding is a node classification problem on the Tanner graph and 2) both GNN and Tanner graph are permutation-invariant due to the linear property of

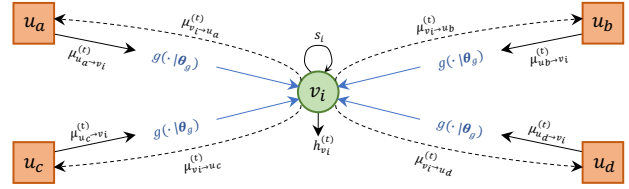


Fig. 5. Illustration of updating the node embedding in the GNN-based decoder. The variable node v_i receives messages from $\mathcal{M}(v_i) = \{u_a, u_b, u_c, u_d\}$. $g(\cdot | \theta_g)$ is a trainable neural network.

codes [27, Section 2]. In this section, we propose an EW-GNN decoder operating on the Tanner graph, which is different from the lattice graph used by DRL code designer in Section III.

A. GNN Decoder with Edge Weights

Considering a bipartite Tanner graph $\mathcal{G} = (\mathcal{V}, \mathcal{U}, \mathcal{E})$ with directed edge messages, as introduced in Section II-A2, we define the node feature of variable node v_i as the received LLR information¹, ℓ_i given by (2). In each iteration, the hidden node embedding of v_i , denoted as $h_{v_i}^{(t)}$, is updated based on incoming edge messages $\mu_{u \rightarrow v}^{(t)}$, which is iteratively generated from $\mu_{v \rightarrow u}^{(t-1)}$. Figure 5 gives an example of the updating process. Since n variable nodes correspond to n codeword bits, the GNN decoder finally obtains \hat{c}_i from $h_{v_i}^{(T)}$, for $v_i \in \mathcal{V}$, after T iterations.

In the proposed GNN decoder, we introduce “weight” to the edge messages to improve the decoding performance. Intuitively, by reducing the weights of unreliable edge messages generated from small cycles in the Tanner graph, it is possible to improve the accuracy of the output codeword estimate \hat{c} .

The weight is a multiplicative correction factor [43] working on the edge message from parity-check nodes to variable nodes. Let us denote the weight of $\mu_{u_j \rightarrow v_i}^{(t)}$ in the t -th iteration as $w_{u_j \rightarrow v_i}^{(t)} \in \mathbb{R}$. By employing an MLP, $g(\cdot | \theta_g)$ with trainable parameters θ_g , the weight $w_{u_j \rightarrow v_i}^{(t)}$ is learned from input features that can reflect the reliability of node and edge information, which is defined as

$$w_{u_j \rightarrow v_i}^{(t)} = g(|\mu_{u_j \rightarrow v_i}^{(t)}|, \delta^{(t)}(\mu_{u_j \rightarrow v_i}), \delta^{(t-1)}(\mu_{v_i \rightarrow u_j}), \delta^{(t-1)}(h_{v_i}) | \theta_g). \quad (19)$$

In (19), $|\mu_{u_j \rightarrow v_i}^{(t)}|$ represents the reliability of edge message $\mu_{u_j \rightarrow v_i}^{(t)}$, because $\mu_{u_j \rightarrow v_i}^{(t)}$ can be regarded as an extrinsic LLR (see [29]). Then, $\delta^{(t)}(x)$ is a residual function given by

$$\delta^{(t)}(x) = |x^{(t)} - x^{(t-1)}|. \quad (20)$$

Thus, $\delta^{(t)}(\mu_{u_j \rightarrow v_i})$, $\delta^{(t-1)}(\mu_{v_i \rightarrow u_j})$, and $\delta^{(t-1)}(h_{v_i})$ represent the residual value of $\mu_{u_j \rightarrow v_i}$, $\mu_{v_i \rightarrow u_j}$, and h_{v_i} , respectively. They are also measurements of the reliabilities [44]; precisely, a lower residual value is, a more reliable node/edge will be.

Next, we explain the algorithm of EW-GNN with the help of weight $w_{u_j \rightarrow v_i}^{(t)}$. At the t -th iteration, EW-GNN first updates the edge message from u_j to v_i according to

$$\mu_{u_j \rightarrow v_i}^{(t)} = \ln \frac{\text{clip}\left(1 + \prod_{v \in \mathcal{M}(u_j) \setminus v_i} \tanh\left(\frac{\mu_{v \rightarrow u_j}^{(t-1)}}{2}\right), \alpha, 2 - \alpha\right)}{\text{clip}\left(1 - \prod_{v \in \mathcal{M}(u_j) \setminus v_i} \tanh\left(\frac{\mu_{v \rightarrow u_j}^{(t-1)}}{2}\right), \alpha, 2 - \alpha\right)} \quad (21)$$

¹GNN can apply different update and message functions as per applications. In the GNN decoder, the node classification only performs on variable nodes representing codeword bits. Thus, we only assign features and embeddings to variable nodes for simplicity.

where α is a model parameter less than 10^{-7} . We note that the message update function (3) in BP is not applicable to neural-network-based decoders, because $\tanh^{-1}(\cdot)$ is unbounded and introduces non-differentiable singularities, leading to a non-convergence training process. Therefore, we modify $\tanh^{-1}(\cdot)$ with the clip function to avoid the aforementioned issue. Compared to the Taylor series expansion of $\tanh^{-1}(\cdot)$ used in [16], the clip function in (21) introduces virtually no extra complexity.

After $\mu_{u_j \rightarrow v_i}^{(t)}$ is obtained for $u_j \in \mathcal{U}$ and $v_i \in \mathcal{M}(u_j)$, the updated edge message from v_i to u_j is given by²

$$\mu_{v_i \rightarrow u_j}^{(t)} = \ell_i + \sum_{u \in \mathcal{M}(v_i) \setminus u_j} w_{u \rightarrow v_i}^{(t)} \cdot \mu_{u \rightarrow v_i}^{(t)}. \quad (22)$$

Then, the node embedding $h_v^{(t)}$ is updated by aggregating weighted edge messages from all neighbor nodes according to

$$h_{v_i}^{(t)} = \ell_i + \sum_{u \in \mathcal{M}(v_i)} w_{u \rightarrow v_i}^{(t)} \cdot \mu_{u \rightarrow v_i}^{(t)}. \quad (23)$$

At $t = 0$, the node embeddings $h_{v_i}^{(0)}$ and edge messages $\mu_{v_i \rightarrow u}^{(0)}$ are all initialized to corresponding input features of node v_i , i.e., ℓ_i given in (2). Also, all residuals are initialized to 0. Meanwhile, at the t -th iteration, EW-GNN uses node embeddings and edge messages propagated from previous two iterations to update $h_{v_i}^{(t)}$.

After T iterations, we obtain the estimated codeword $\hat{\mathbf{c}}$ from the node embedding h_{v_i} according to the following rule:

$$\hat{c}_i = \begin{cases} 1, & h_{v_i}^{(T)} \leq 0, \\ 0, & h_{v_i}^{(T)} > 0. \end{cases} \quad (24)$$

B. Training Algorithm

The algorithm of the proposed EW-GNN decoder is summarized in Algorithm 6, which includes the training phase and the inference phase. The goal of the training phase is to find an optimal $g(\cdot | \theta_g)$ that minimizes the difference between the transmitted codeword and its estimate. For channel coding, a large amount of data samples can be easily obtained to perform the end-to-end training [13]. The label data, i.e., the transmitted codewords, are generated by encoding a random binary message. By imposing an AWGN with power σ_n^2 over the symbols of codewords, received LLRs can be computed according to (2), which are used as the input data of EW-GNN. To improve the robustness of EW-GNN, we perform the training process with diverse SNRs uniformly distributed in the interval $[\gamma_{\min}, \gamma_{\max}]$.

Since the channel decoding can be considered as a bit-wise binary classification task, we apply the average binary cross-entropy (BCE) per bit per iteration as the loss function, i.e.,

$$L = -\frac{1}{nT} \sum_{t=1}^T \sum_{i=1}^n c_i \log(p_{v_i}^{(t)}) + (1 - c_i) \log(1 - p_{v_i}^{(t)}), \quad (25)$$

which is the multiloss variant [15] of a regular BCE loss function. In (25), $p_{v_i}^{(t)}$ denotes the probability $\Pr(c_i = 1)$ estimated from $h_{v_i}^{(t)}$ of v_i at iteration t , which is given by $p_{v_i}^{(t)} = 1/(1 + \exp(h_{v_i}^{(t)})) \in (0, 1)$. During the training phase, $g(\cdot | \theta_g)$ parameters are updated utilizing the Adam optimizer with a given learning rate η [42], and L_{n_B} in Algorithm 6 is the loss of the n_B -th sample in the batch of size N_B .

² $M_t(\mu_{u_j \rightarrow v_i}^{(t)}, h_{v_i}^{(t-1)}) = w_{u_j \rightarrow v_i}^{(t)} \mu_{u_j \rightarrow v_i}^{(t)}$ as $w_{u_j \rightarrow v_i}^{(t)}$ is a function of $h_{v_i}^{(t-1)}$.

Algorithm 6: Training and Inference of EW-GNN

▷ Training Phase:

Input : \mathbf{G}, \mathbf{H} , training batch size N_B , training SNR $[\gamma_{\min}, \gamma_{\max}]$, number of iterations T , learning rate η

Output: well-trained $g^*(\cdot | \theta_g^*)$

```

1 Create the network topology,  $\mathcal{G} = (\mathcal{V}, \mathcal{U}, \mathcal{E})$  from  $\mathbf{H}$ ;
2 foreach epoch do
3   for  $n_B \leftarrow 1 : N_B$  do
4     Encode a random message  $\mathbf{b}$  to  $\mathbf{c} = \mathbf{bG}$ ;
5     Obtain the noisy signal  $\mathbf{y}$  with the AWGN channel
      at a random SNR  $\gamma \in [\gamma_{\min}, \gamma_{\max}]$ ;
6     Obtain the received LLR vector  $\ell$  by (2);
7     Initialize  $h_{v_i}^{(0)} = \ell_i$ ,  $\mu_{v_i \rightarrow u}^{(0)} = \ell_i$ ,  $\mu_{u \rightarrow v}^{(0)} = 0$ ,  $\delta^{(0)}(\cdot) = 0$ ;
8     for  $t \leftarrow 1 : T$  do
9       foreach  $e_{i,j} \in \mathcal{E}$  do
10        Update edge message  $\mu_{u_j \rightarrow v_i}^{(t)}$  by (21);
11        Update weight  $w_{u_j \rightarrow v_i}^{(t)}$  by (19);
12        Update edge message  $\mu_{v_i \rightarrow u_j}^{(t)}$  by (22);
13      end
14      foreach  $v_i \in \mathcal{V}$  do
15        Update node embedding  $h_{v_i}^{(t)}$  by (23);
16      end
17    endfor
18    Calculate the multiloss value  $L_{n_B}$  by (25);
19  endfor
20  Update  $\theta_g$  with the loss  $L(\theta_g) = \frac{1}{N_B} \sum_{n_B=1}^{N_B} L_{n_B}$ ;
21 end
    
```

▷ Inference Phase:

Input : LLRs of the received codewords $\ell \in \mathbb{R}^n$, parity-check matrix \mathbf{H}' , number of iterations T'

Output: estimated codewords $\hat{\mathbf{c}}$

```

22 Create the network topology,  $\mathcal{G}' = (\mathcal{V}', \mathcal{U}', \mathcal{E}')$  from  $\mathbf{H}'$ ;
23 Execute lines 7-17 on  $\mathcal{G}'$  with  $g^*(\cdot | \theta_g^*)$  for  $T'$  iterations;
24 Obtain the estimated codewords  $\hat{\mathbf{c}}$  according to (24).
    
```

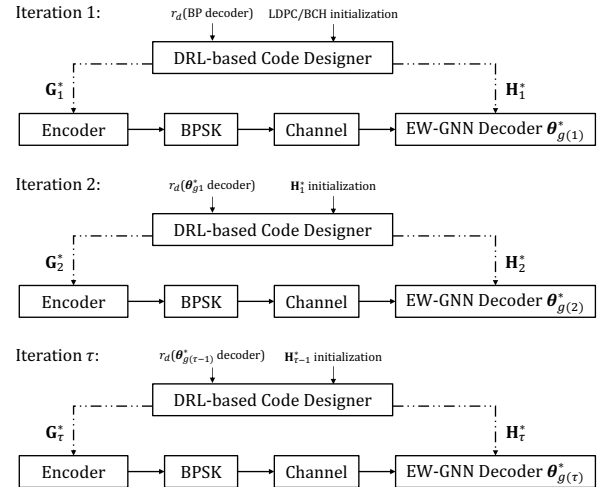


Fig. 6. The iterative training phase of the proposed GNN-DRL auto-encoder architecture with τ training iterations.

V. AUTO-ENCODER WITH ITERATIVE TRAINING

An auto-encoder framework for linear block code provides a communication scheme in which both the encoder and the decoder are implemented by machine learning methods, and they can be optimized jointly. In our auto-encoder model, the DRL-based code designer generates an optimal code with an initial decoder, e.g., BP. The EW-GNN decoder is then

trained based on this code. Subsequently, the DRL-based code designer generates a new optimal code with the trained EW-GNN decoder, and the EW-GNN decoder is fine-tuned based on the new code. The encoder and decoder will be trained in this manner for several iterations. We employ this iterative training method because the direct joint optimization of a DRL-based model and a supervised learning-based model is difficult due to the vast combined parameter space of two models. On the other hand, the reward-based, unsupervised-learned DRL code designer and the loss-based, supervised-learned EW-GNN decoder have completely different training processes.

The detailed iterative training process of the proposed auto-encoder framework is illustrated in Fig. 6. At the first iteration, a DRL-based code designer is independently trained using the BER reward measured by BP decoding and outputs the learned code \mathbf{H}_1^* . Conventional linear block codes, such as LDPC and BCH, are chosen as the state initialization matrices at the first iteration. The EW-GNN decoder is then trained based on \mathbf{H}_1^* and its corresponding generator matrix \mathbf{G}_1^* according to Algorithm 6, providing a well-trained decoder network, which can be represented by its parameters $\theta_{g(1)}$. In the second training iteration, the $\theta_{g(1)}$ decoder is employed to measure the decoding BER reward, and the state of the DRL-based code designer is initialized as \mathbf{H}_1^* . Then, the code designer generates \mathbf{H}_2^* , which are used to train a new EW-GNN decoder $\theta_{g(2)}$. This training process is iteratively repeated for a few iterations.

After τ iterations, our auto-encoder framework produces an expertly designed linear block code represented by \mathbf{H}_τ^* , accompanied by an optimally trained EW-GNN decoder with parameters $\theta_{g(\tau)}$. These components can be jointly employed to assemble a channel coding system with superior error-control capabilities. Our auto-encoder has offline generation of codes and associated decoders, as the on-the-fly design of codes is impractical due to the extensive complexity DRL model training. Once the auto-encoder generates an optimal linear block code from the DRL-based code designer, \mathbf{H}_τ^* and \mathbf{G}_τ^* can be stored to enable fast online encoding by (1) and fast online decoding by executing the inference phase in Algorithm 6. The EW-GNN algorithm has a low inference complexity that increases linearly with the code length [20]; thus, its decoding complexity is similar to BP.

Our auto-encoder framework guides the code matrix design based on a trainable decoding method, allowing the encoder and decoder to reciprocally train toward optimal performance; Moreover, the state initialization and the reward function are continuously updated, improving the exploration efficiency.

VI. EXPERIMENTS AND RESULTS

This section presents the results obtained from our proposed algorithms. We first evaluate the performance of the DRL-based code designer and the EW-GNN decoder separately. For the code designer, we examine the BER performance of the learned codes, by using them to encode messages over AWGN channel with BP and MLD decoders. Meanwhile, the BER performance of the proposed EW-GNN decoder is evaluated by using it to decode classic analytically designed codes. Subsequently, we will demonstrate the performance of the proposed auto-encoder framework. All BER results are measured at each SNR by performing simulations until

TABLE I
HYPER-PARAMETERS OF THE PROPOSED DRL-BASED CODE DESIGNER

Parameters	Value	
Environment	State initialization \mathbf{S}^1	CCSDS (32, 16) LDPC
	Flipping threshold α_f	0.3
	\mathbf{A}^t range $[\alpha_{\text{low}}, \alpha_{\text{high}}]$	[0, 1]
	Step number T_c	25
BER reward	Decoding method	BP with 8 iterations
	Decoding SNR	6 dB
Structure reward	α_d	8
	α_c	500
MPMNN	Embedding dimension d_e	10
	Message dimension	10
	MPMNN layers	3
	MLP layers	3
Noise	MLP hidden units	40
	Gaussian noise factor σ_ϵ	0.3
Training	Learning rates η_a and η_c	0.001
	Discount factor γ	0.99
	Target update factor ρ	0.001
	Batch size N_B	128

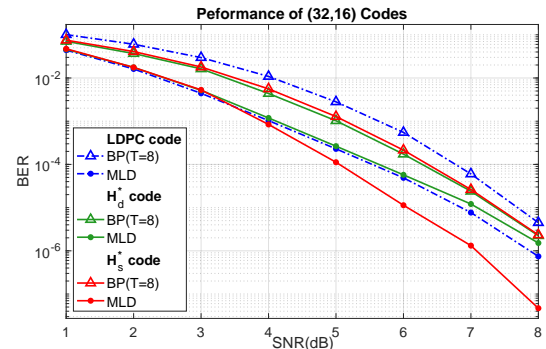


Fig. 7. BER performance for designed (32, 16) linear block codes.

10,000 bit errors are collected. For different coding schemes, we define *coding gain* as the difference in SNRs required to achieve the same target BER at high SNRs.

A. DRL-based Neural Code Designer

We evaluate the BER of the codes generated by our DRL-based code designer, as outlined in Algorithm 5. We employ two different types of reward functions to generate two distinct codes \mathbf{H}_d^* and \mathbf{H}_s^* . Specifically, \mathbf{H}_d^* is produced using the decoding BER reward in (7) with a 8-iteration BP decoder over 6 dB AWGN, and \mathbf{H}_s^* is produced using the code structure reward in (8). Their BER performance is evaluated with the BP decoder with 8 iterations and MLD. BP is an efficient suboptimal decoder designed for LDPC codes, while MLD can fully exploit the error-correction capability of any codes. This approach allows us to test the designed codes under both optimal and suboptimal decoders. The training algorithm of the DRL-based code designer is implemented using TensorFlow, with hyper-parameters detailed in Table I.

As illustrated in Fig. 7, the DRL-based code designer generates \mathbf{H}_d^* and \mathbf{H}_s^* with parameters $k = 16, n = 32$ and they are compared with the traditional CCSDS (32, 16) LDPC [45]. As shown, both \mathbf{H}_d^* and \mathbf{H}_s^* , can achieve better BER performance than the LDPC code. When decoded by BP, \mathbf{H}_d^* achieves the best decoding performance among all

TABLE II
CODE PROPERTIES OF DESIGNED (32, 16) LINEAR BLOCK CODES

Code properties	LDPC	\mathbf{H}_d^*	\mathbf{H}_s^*
MHD	4	3	5
Number of 4-cycles	178	52	72
Number of 6-cycles	2090	487	685
Density	0.250	0.186	0.193
BER with BP at 5dB	$2.81e-3$	$1.03e-3$	$1.28e-3$
BER with ML at 5dB	$2.29e-4$	$2.64e-4$	$1.12e-4$

TABLE III
HYPER-PARAMETERS OF THE PROPOSED EW-GNN DECODER

Parameters	BCH codes	LDPC codes
Clip factor α	10^{-32}	10^{-7}
SNR range $[\gamma_{\min}, \gamma_{\max}]$	[3 dB, 8 dB]	[1 dB, 8 dB]
Batch size N_B	2000	4000
Learning rate η	$10^{-3} \sim 10^{-5}$	
Number of iterations T	8	
MLP layers	3	
MLP hidden units	32	
ELU factor β	1.0	

the counterparts, and has 0.65 dB more coding gain than the LDPC code at high SNRs around 6 dB. Although the decoding BER reward value is measured only at the SNR of 6 dB, the learned \mathbf{H}_d^* demonstrates superior performance over a wide range of SNRs. Under MLD, \mathbf{H}_s^* achieves better BER performance than LDPC, with an increased coding gain of 0.83 dB at higher SNRs. This validates the performance of the proposed DRL-based code designer in learning good codes with superior error-correction capability.

We further examine the algebraic structure properties of these (32, 16) codes, as presented in Table II. As shown in the table, the MHD of the DRL-generated matrices \mathbf{H}_d^* and \mathbf{H}_s^* are 3 and 5, respectively, while the CCSDS (32, 16) LDPC code has an MHD of 4. As a result, \mathbf{H}_d^* exhibits inferior performance compared to the LDPC code when decoded using the MLD, while \mathbf{H}_s^* allows an excellent MLD performance. Table II also demonstrates that the density of these parity-check matrices and the number of short cycles in their associated Tanner graphs. Compared to the benchmark LDPC, the learned \mathbf{H}_d^* and \mathbf{H}_s^* are both more sparse and have less number of cycles of length 4. Consequently, both \mathbf{H}_d^* and \mathbf{H}_s^* outperform the LDPC code under the BP decoding.

We note that the BP-decoding BER reward function tends to produce matrices with fewer short cycles and lower density, but this leads to poor MHD performance of \mathbf{H}_d^* . This can be addressed by the auto-encoder framework proposed in Section V, whose performance will be demonstrated in Section VI-C.

B. EW-GNN Decoder

In this subsection, we evaluate the error-correction performance and the scalability of the proposed EW-GNN for short BCH codes and LDPC codes. The BP and NBP decoders [15] are considered as benchmarks for performance comparison. The decoding performance of these algorithms is measured by BER at various SNRs. The training of the EW-GNN algorithm is implemented using TensorFlow with hyper-parameters in Table III.

1) *BCH Codes*: We first train an EW-GNN decoder for the (63, 51) BCH code with $T = 8$ decoding iterations, and consider two inference scenarios with different number of decoding iterations, $T = 8$ and $T = 30$.

As shown in Fig. 8a, EW-GNN outperforms BP and NBP in terms of BER for (63, 51) BCH code with both $T = 8$ and $T = 30$. When $T = 8$, our proposed EW-GNN decoder has 1.2 dB and 0.62 dB larger coding gains compared to the BP and NBP algorithms, respectively, at high SNRs. Although EW-GNN is trained in the scenario with $T = 8$, its BER performance remains superior with a larger number of decoding iterations. As shown, when $T = 30$, the EW-GNN decoder outperforms the NBP decoder by 0.61 dB. It is worth noting that our proposed decoder with $T = 8$ has a better BER performance than the NBP decoder with $T = 30$.

We directly apply the EW-GNN model trained for the (63, 51) BCH code with $T = 8$ to decode (63, 45) and (63, 36) BCH codes. Note that the Tanner graph of (63, 51) BCH codes has much fewer edges (i.e., smaller network size) than those of (63, 45) and (63, 36) BCH codes. As can be seen in Figs. 8b and 8c, the EW-GNN algorithm still achieves better BER performance than the BP and NBP algorithms for (63, 45) and (63, 36) BCH codes. For example, when decoding the (63, 36) BCH code with $T = 30$, the proposed EW-GNN increases the coding gain by 0.8 dB and 0.2 dB compared to BP and NBP respectively.

2) *LDPC Codes*: We train the EW-GNN decoder for the half-rate CCSDS (32, 16) LDPC code [45] with the number of decoding iterations $T = 8$. As depicted in Fig. 9a, the proposed EW-GNN algorithm achieves the best decoding performance among all its counterparts in decoding the (32, 16) LDPC code. Specifically, when $T = 30$, EW-GNN improves the coding gains of BP and NBP by 0.21 dB and 0.1 dB at high SNRs, respectively.

To investigate the scalability of EW-GNN to different code lengths, the EW-GNN model trained for the (32, 16) LDPC codes is directly applied to longer LDPC codes at the same code rate. As shown in Fig. 9b, when $n = 128$, the EW-GNN decoder still outperforms the BP decoder and the NBP decoder in terms of BER. Furthermore, when $n = 256$ as illustrated in Fig. 9c, EW-GNN outperforms BP and NBP by 0.3 dB and 0.2 dB of the coding gain at high SNRs, respectively. Therefore, we highlight that even though EW-GNN is trained with an extremely short code ($n = 32$), it can achieve better BER performance when applied to longer codes without fine-tuning.

3) *High-Scalability Performance*: As shown in Figs. 8-9, the EW-GNN scheme exhibits significant scalability, allowing a decoder trained on one code to be used for another without retraining. By leveraging the message-passing structure [36], the EW-GNN decoder learns at nodes from the immediate local neighborhood information and the hidden parameters shared by all edges in the Tanner graph. Thus, the number of trainable parameters is independent of input graph size. The EW-GNN decoder offers a versatile and efficient solution for decoding linear block codes of varying lengths, reducing the need for retraining and adapting to different code lengths. The ability to generalize from short to long codes ensures that EW-GNN can maintain high performance across different

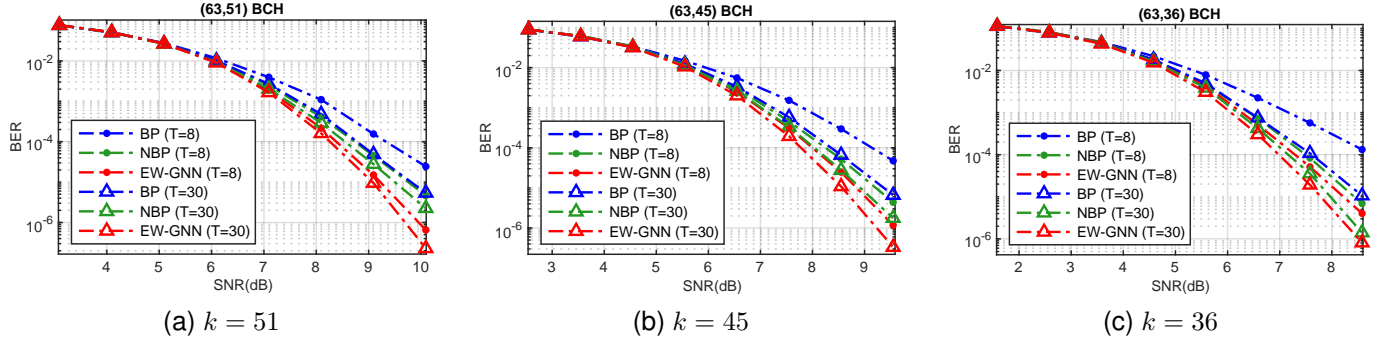


Fig. 8. BER performance for BCH codes of length $n = 63$. EW-GNN is only trained with the (63, 51) BCH code and $T = 8$.

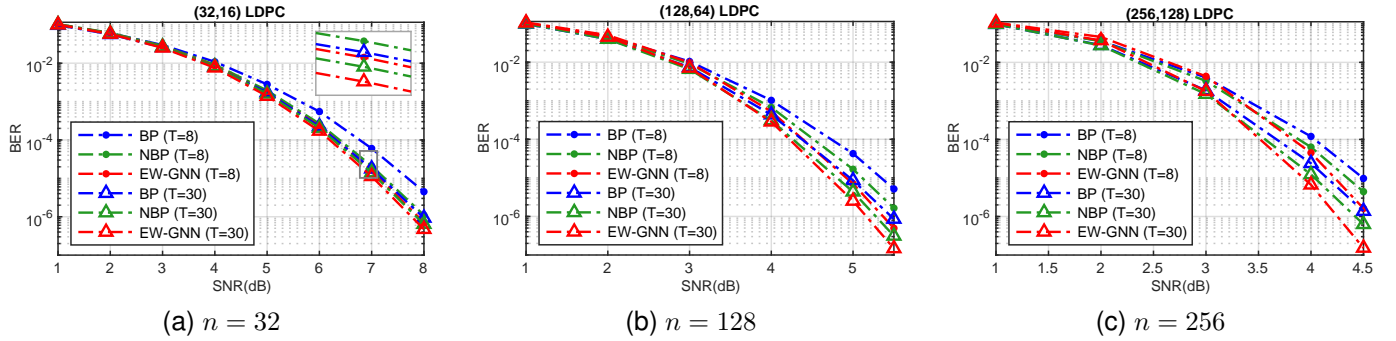


Fig. 9. BER performance for LDPC codes at rate 1/2. EW-GNN is only trained with the (32, 16) LDPC code and $T = 8$.

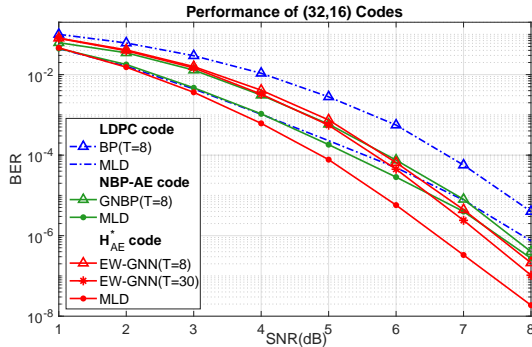


Fig. 10. BER performance for designed (32, 16) linear block codes. \mathbf{H}_{AE}^* code is generated by our auto-encoder scheme with three training iterations.

coding scenarios, making them suitable for a wide range of applications in wireless communications.

C. GNN-DRL Auto-encoder

We first evaluate the performance of the proposed auto-encoder framework by training it on a (32, 16) code and compare it to the LDPC code. Next, we extend the application of the auto-encoder model to a (63, 45) code and compare its performance against a standard BCH code. Finally, we analyze the impact of its individual components of encoder and decoder separately, and elucidate how the iterative training procedure enhances the performance of auto-encoder.

1) (32, 16) Codes: We first train an auto-encoder model with $\tau = 3$ training iterations to produce (32, 16) codes. Two benchmarks are considered for comparison: the CCSDS (32, 16) LDPC code paired with the BP decoder, and the NBP-AE [21]. NBP-AE is equipped with the Gated Neural Belief Propagation (GNBP) decoder, which is an improved trainable

version of BP. All these decoders, BP, GNBP, and our EW-GNN, are iterative message-passing decoders implemented with 8 decoding iterations. In the DRL-based code designer, the parity-check matrix of the CCSDS (32, 16) LDPC is utilized as the state initialization matrix. As depicted in Fig. 10, our auto-encoder outperforms the traditional LDPC coding system by a coding gain of 1 dB under message-passing decoding. Additionally, when compared with the NBP-AE system, our model shows a coding gain of approximately 0.21 dB at high SNRs. This coding gain can be attributed to the reduced number of short cycles in the Tanner graph of the code generated by our DRL-based code designer. Specifically, the code generated by our auto-encoder after 3 training iterations, denoted by \mathbf{H}_{AE}^* , has only 77 4-step cycles, which is significantly fewer than 172 short cycles in the code designed by NBP-AE. Furthermore, in the proposed auto-encoder, we can directly apply the trained EW-GNN decoder to the designed code with a larger number of decoding iterations than that used in training. As shown in Fig. 7, by increasing the number of EW-GNN decoding iterations to 30, we can achieve a 0.22 dB further gain compared to using an 8-iteration EW-GNN decoder.

We also test the MLD performance of all these (32, 16) codes. Despite our auto-encoder model being trained to minimize the EW-GNN decoding BER, generated codes also demonstrate robust BER performance under MLD. Notably, our \mathbf{H}_{AE}^* code has coding gains of 1.28 dB and 0.93 dB over the CCSDS LDPC code and the (32, 16) NBP-AE code, respectively, at high SNRs. Moreover, the proposed auto-encoder is capable of reconciling the decoding efficiency achieved by a suboptimal decoder (e.g., iterative decoding) with the decoding performance achieved by an optimal decoder (e.g., MLD). For

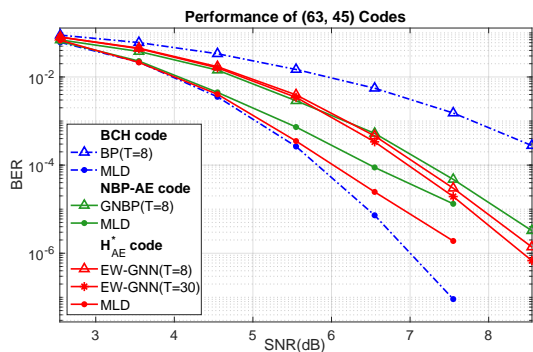


Fig. 11. BER performance for designed (63, 45) linear block codes. \mathbf{H}_{AE}^* code is generated by our auto-encoder scheme with three training iterations.

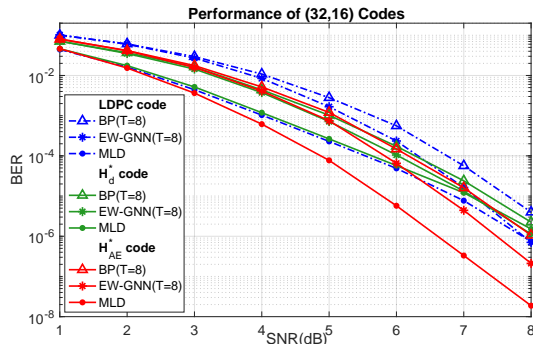


Fig. 12. Evaluate the relative contributions of the DRL-based code designer and the EW-GNN decoder.

example, when using the EW-GNN decoder with $T = 30$ iterations for \mathbf{H}_{AE}^* , it achieves a BER that is superior to the MLD performance of LDPC for SNRs above 6 dB, with a coding gain of up to 0.63 dB.

2) (63, 45) Codes: We also train an auto-encoder model using the parity-check matrix of the (63, 45) BCH [39] as the state initialization. As depicted in Fig. 11, the proposed auto-encoder, i.e., the learned (63, 45) \mathbf{H}_{AE}^* with its associated EW-GNN decoder, is compared with the (63, 45) BCH paired with BP and the (63, 45) NBP-AE system [21]. Our auto-encoder scheme significantly outperforms the standard BCH with BP and the neural NBP-AE system, achieving coding gains of up to 1.81 dB and 0.28 dB at high SNRs, respectively.

Figure 11 presents the BER of MLD for all these (63, 45) codes. However, unlike the case of (32, 16) codes, the MLD performance of the learned code is worse than that of the BCH code. This is reasonable because the BCH code is the best-known linear code with the highest MHD compared with all other existing codes. Under MLD, the BCH code can achieve the normal approximation bound [1] at this short block length. In addition, our auto-encoder model is specifically trained to optimize coding performance with the EW-GNN decoder, rather than the MLD. The learning process tends to generate matrices with lower density and fewer short cycles, which is ideal for BP and EW-GNN to achieve an acceptable performance-complexity trade-off.

3) *Impact of each Components:* In Fig. 12, we analyze the impact of various elements over the performance of the auto-encoder by comparing different code-decoder pairs of (32, 16). In the figure, \mathbf{H}_{AE}^* is the code produced by our auto-encoder scheme with three training iterations, while \mathbf{H}_d^* is produced by the DRL-based code designer using BP-decoding BER reward

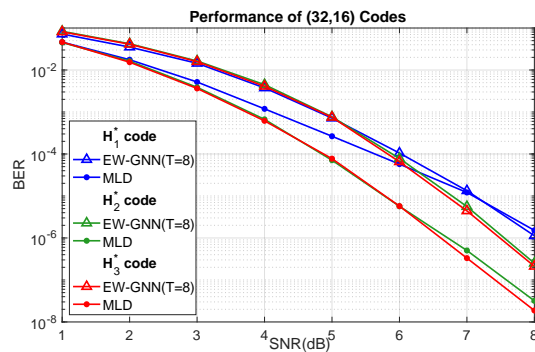


Fig. 13. Evaluate the relative contributions of the iterative training method.

in one-shot training. When applied to \mathbf{H}_{AE}^* , the EW-GNN decoder is iteratively trained in the auto-encoder, while when applied to \mathbf{H}_d^* , the EW-GNN decoder is fine-tuned for \mathbf{H}_d^* .

All the schemes using the code designed from DRL, including \mathbf{H}_{AE}^* and \mathbf{H}_d^* , can achieve better performance than the traditional LDPC with BP. Our auto-encoder model (i.e., \mathbf{H}_{AE}^* with EW-GNN) achieves the best BER performance among all schemes. In addition, the code generated by our auto-encoder framework, \mathbf{H}_{AE}^* , has better BER results than its counterparts, under all three different decoders. Especially, the BER result of the \mathbf{H}_{AE}^* under MLD significantly outperforms that of all other coding schemes with substantial coding gains. Furthermore, as shown in Fig. 12, when replacing the LDPC code with the learned code while still decoding with BP, the BER performance improves primarily at low SNRs. Nevertheless, when comparing EW-GNN to BP in decoding LDPC code, the performance gain is significant only at high SNRs. In contrast, the auto-encoder model can have a superior BER performance under a wide range of SNRs. Therefore, both the trainable code and the trainable EW-GNN contribute to the final outstanding performance of the auto-encoder.

To evaluate the impact of the iterative training procedure, we compare the performances of various auto-encoder models with different numbers of training iterations as demonstrated in Fig. 6. As shown in Fig. 13, \mathbf{H}_2^* significantly outperforms \mathbf{H}_1^* under both EW-GNN decoder and MLD. However, the coding gain between \mathbf{H}_2^* and \mathbf{H}_3^* diminishes, indicating that the performance of both code and decoder has nearly converged to the optimal point. This fast convergence can be attributed to the high scalability of the EW-GNN decoder. As discussed in Section VI-B, EW-GNN exhibits high scalability across various codes. Consequently, different codes as training inputs do not significantly affect the optimality of the EW-GNN decoder. Thus, from the second training iteration onwards, performance gain is primarily contributed by the DRL-based code designer.

VII. CONCLUSION

In this paper, we proposed an innovative auto-encoder framework that leverages GNN and DRL to develop high-performance channel coding schemes for short linear block codes. First, we introduced a DRL-based code designer, where a GNN agent generates the binary parity-check matrix by iteratively flipping its elements. Simulation results demonstrated that the DRL-designed short code exhibit superior BER performance with a 0.83 dB coding gain compared

to the standard LDPC code under MLD. Furthermore, we developed a scalable EW-GNN decoder for short linear block codes. Simulation results show that EW-GNN can improve BER performance compared to the conventional BP and the NBP decoder for short BCH and LDPC codes. For example, when decoding (63, 51) BCH code, the proposed EW-GNN increases the coding gain by 1.2 dB than BP. A well-trained EW-GNN can decode longer or more complex codes without retraining, enabling its application in practical communication systems with dynamic code lengths. Finally, the GNN-DRL auto-encoder integrates the DRL-based code designer and the EW-GNN decoder through an iterative joint training process, ensuring simultaneous optimization of both the encoder and decoder. Simulations show that our proposed auto-encoder framework achieves better BER results than multiple traditional coding systems and the NBP-AE from the literature, while keeping the low decoding complexity similar to that of BP. Particularly, our auto-encoder system can achieve a coding gain of 0.63 dB compared to the standard (32, 16) LDPC with MLD.

REFERENCES

- [1] M. Shirvanimoghaddam, M. S. Mohammadi, R. Abbas, A. Minja, C. Yue, B. Matuz, G. Han, Z. Lin, W. Liu, Y. Li, S. Johnson, and B. Vucetic, "Short block-length codes for ultra-reliable low latency communications," *IEEE Commun. Mag.*, vol. 57, no. 2, pp. 130–137, Feb. 2019.
- [2] C. Yue, V. Miloslavskaya, M. Shirvanimoghaddam, B. Vucetic, and Y. Li, "Efficient decoders for short block length codes in 6g urllc," *IEEE Commun. Mag.*, vol. 61, no. 4, pp. 84–90, Apr. 2023.
- [3] "NR; Multiplexing and channel coding (Release 16), v16.0.0," 3rd Generation Partnership Project (3GPP), Tech. Rep. TS 38.212, Jan. 2020.
- [4] Y. Polyanskiy, H. V. Poor, and S. Verdú, "Channel coding rate in the finite blocklength regime," *IEEE Trans. Inf. Theory*, vol. 56, no. 5, pp. 2307–2359, May 2010.
- [5] Q. Mao, F. Hu, and Q. Hao, "Deep learning for intelligent wireless networks: A comprehensive survey," *IEEE Commun. Surv. Tutor.*, vol. 20, no. 4, pp. 2595–2621, 4th Quart. 2018.
- [6] L. Dai, R. Jiao, F. Adachi, H. V. Poor, and L. Hanzo, "Deep learning for wireless communications: An emerging interdisciplinary paradigm," *IEEE Wireless Commun.*, vol. 27, no. 4, pp. 133–139, Aug. 2020.
- [7] N. Samuel, T. Diskin, and A. Wiesel, "Deep mimo detection," in *Proc. IEEE SPAWC*, 2017, pp. 1–5.
- [8] H. Sun, X. Chen, Q. Shi, M. Hong, X. Fu, and N. D. Sidiropoulos, "Learning to optimize: Training deep neural networks for wireless resource management," in *Proc. IEEE SPAWC*, 2017, pp. 1–6.
- [9] Y. Jiang, H. Kim, H. Asnani, S. Kannan, S. Oh, and P. Viswanath, "Learn codes: Inventing low-latency codes via recurrent neural networks," in *Proc. IEEE ICC*, 2019, pp. 1–7.
- [10] H. Kim, Y. Jiang, S. Kannan, S. Oh, and P. Viswanath, "Deepcode: Feedback codes via deep learning," *IEEE J. Sel. Areas Inf. Theory*, vol. 1, no. 1, pp. 194–206, May 2020.
- [11] M. Ebada, S. Cammerer, A. Elkelesh, and S. ten Brink, "Deep learning-based polar code design," in *Proc. IEEE Annu. Allerton Conf. Commun. Control Comput.*, 2019, pp. 177–183.
- [12] L. Huang, H. Zhang, R. Li, Y. Ge, and J. Wang, "Ai coding: Learning to construct error correction codes," *IEEE Trans. Commun.*, vol. 68, no. 1, pp. 26–39, Jan. 2020.
- [13] T. Gruber, S. Cammerer, J. Hoydis, and S. t. Brink, "On deep learning-based channel decoding," in *Proc. IEEE CISS*, 2017, pp. 1–6.
- [14] E. Nachmani, Y. Be'ery, and D. Burshtein, "Learning to decode linear codes using deep learning," in *Proc. IEEE Annu. Allerton Conf. Commun. Control Comput.*, 2016, pp. 341–346.
- [15] E. Nachmani, E. Marciano, L. Lugosch, W. J. Gross, D. Burshtein, and Y. Be'ery, "Deep learning methods for improved decoding of linear codes," *IEEE J. Sel. Topics Signal Process.*, vol. 12, no. 1, pp. 119–131, Feb. 2018.
- [16] E. Nachmani and L. Wolf, "Hyper-graph-network decoders for block codes," in *Proc. NeurIPS*, 2019, pp. 2326–2336.
- [17] A. Buchberger, C. Häger, H. D. Pfister, L. Schmalen, and A. Graell i Amat, "Pruning and quantizing neural belief propagation decoders," *IEEE J. Sel. Areas Commun.*, vol. 39, no. 7, pp. 1957–1966, Jul. 2021.
- [18] E. Nachmani and Y. Be'ery, "Neural decoding with optimization of node activations," *IEEE Commun. Lett.*, vol. 26, no. 11, pp. 2527–2531, Nov. 2022.
- [19] S. Cammerer, J. Hoydis, F. A. Aoudia, and A. Keller, "Graph neural networks for channel decoding," in *Proc. IEEE GC Wkshps*, 2022, pp. 486–491.
- [20] K. Tian, C. Yue, C. She, Y. Li, and B. Vucetic, "A scalable graph neural network decoder for short block codes," in *Proc. IEEE ICC*, 2023, pp. 1268–1273.
- [21] G. Larue, L.-A. Dufrene, Q. Lampin, H. Ghauch, and G. R.-B. Othman, "Neural belief propagation auto-encoder for linear block code design," *IEEE Trans. Commun.*, vol. 70, no. 11, pp. 7250–7264, Nov. 2022.
- [22] T. O'Shea and J. Hoydis, "An introduction to deep learning for the physical layer," *IEEE Trans. Cogn. Commun. Netw.*, vol. 3, no. 4, pp. 563–575, Dec. 2017.
- [23] H. Ye, L. Liang, and G. Y. Li, "Circular convolutional auto-encoder for channel coding," in *Proc. IEEE SPAWC*, 2019, pp. 1–5.
- [24] Y. Jiang, H. Kim, H. Asnani, S. Kannan, S. Oh, and P. Viswanath, "Turbo autoencoder: Deep learning based channel codes for point-to-point communication channels," in *Proc. NeurIPS*, vol. 32, 2019.
- [25] E. Balevi and J. G. Andrews, "Autoencoder-based error correction coding for one-bit quantization," *IEEE Trans. Commun.*, vol. 68, no. 6, pp. 3440–3451, Jun. 2020.
- [26] D. L. Donoho *et al.*, "High-dimensional data analysis: The curses and blessings of dimensionality," *AMS Math. Chall. Lect.*, vol. 1, no. 2000, p. 32, 2000.
- [27] K. Xu, J. Li, M. Zhang, S. S. Du, K. ichi Kawarabayashi, and S. Jegelka, "What can neural networks reason about?" in *Proc. ICLR*, 2020.
- [28] Y. Mao and A. Banihashemi, "A heuristic search for good low-density parity-check codes at short block lengths," in *Proc. IEEE ICC*, vol. 1, 2001, pp. 41–44.
- [29] J. Hagenauer, E. Offer, and L. Papke, "Iterative decoding of binary block and convolutional codes," *IEEE Trans. Inf. Theory*, vol. 42, no. 2, pp. 429–445, Mar. 1996.
- [30] F. Kschischang, B. Frey, and H.-A. Loeliger, "Factor graphs and the sum-product algorithm," *IEEE Trans. Inf. Theory*, vol. 47, no. 2, pp. 498–519, Feb. 2001.
- [31] T. Hehn, J. B. Huber, S. Laendner, and O. Milenkovic, "Multiple-bases belief-propagation for decoding of short block codes," in *Proc. IEEE ISIT*, 2007, pp. 311–315.
- [32] T. P. Lillicrap, J. J. Hunt, A. Pritzel, N. Heess, T. Erez, Y. Tassa, D. Silver, and D. Wierstra, "Continuous control with deep reinforcement learning," in *Proc. ICLR*, 2016.
- [33] D. Silver, G. Lever, N. Heess, T. Degris, D. Wierstra, and M. Riedmiller, "Deterministic policy gradient algorithms," in *Proc. ICML*, vol. 32, PMLR, 2014, pp. 387–395.
- [34] V. Mnih *et al.*, "Human-level control through deep reinforcement learning," *Nature*, vol. 518, no. 7540, pp. 529–533, Feb. 2015.
- [35] Z. Wu, S. Pan, F. Chen, G. Long, C. Zhang, and P. S. Yu, "A comprehensive survey on graph neural networks," *IEEE Trans. Neural Netw. Learn. Syst.*, vol. 32, no. 1, pp. 4–24, Jan. 2021.
- [36] J. Gilmer, S. S. Schoenholz, P. F. Riley, O. Vinyals, and G. E. Dahl, "Neural message passing for quantum chemistry," in *Proc. ICML*, PMLR, 2017, p. 1263–1272.
- [37] Y. Shen, J. Zhang, S. H. Song, and K. B. Letaief, "Graph neural networks for wireless communications: From theory to practice," *IEEE Trans. Wireless Commun.*, vol. 22, no. 5, pp. 3554–3569, May 2023.
- [38] M. Grassl, "Bounds on the minimum distance of linear codes and quantum codes," 2007.
- [39] M. Helmling, S. Scholl, F. Gensheimer, T. Dietz, K. Kraft, S. Ruzika, and N. Wehn, "Database of Channel Codes and ML Simulation Results," www.uni-kl.de/channel-codes, 2019.
- [40] M. Karimi and A. H. Banihashemi, "Message-passing algorithms for counting short cycles in a graph," *IEEE Trans. Commun.*, vol. 61, no. 2, pp. 485–495, Feb. 2013.
- [41] R. S. Sutton and A. G. Barto, *Reinforcement learning: An introduction*. MIT press, 2018.
- [42] D. P. Kingma and J. Ba, "Adam: A method for stochastic optimization," in *Proc. ICLR*, 2015.
- [43] M. Yazdani, S. Hemati, and A. Banihashemi, "Improving belief propagation on graphs with cycles," *IEEE Commun. Lett.*, vol. 8, no. 1, pp. 57–59, Jan. 2004.
- [44] X. Liu, Z. Zhou, R. Cui, and E. Liu, "Informed decoding algorithms of ldpc codes based on dynamic selection strategy," *IEEE Trans. Commun.*, vol. 64, no. 4, pp. 1357–1366, Apr. 2016.
- [45] "Short block length LDPC codes for TC synchronization and channel coding," Consultative Committee for Space Data Systems (CCSDS), Tech. Rep. 231.1-O-1, Apr. 2015.